Fluorescence Lifetime Imaging of NAD(P)H Distinguishes Pathways of Metabolic Inhibition

By

Joseph Thomas Sharick

Thesis
Submitted to the Faculty of the
Graduate School of Vanderbilt University
in partial fulfillment of the requirements
for the degree of

MASTER OF SCIENCE
in

Biomedical Engineering
May, 2016
Nashville, Tennessee

Approved:

Melissa C. Skala, Ph.D.
H. Charles Manning, Ph.D.

ACKNOWLEDGEMENTS

I would like to thank the funding sources that supported this project, including the NSF Graduate Research Fellowship (DGE-1445197), the DOD Breast Cancer Research Program (DOD-BC121998), and the NIH (NCI R01 CA185747).

I would also like to thank Teresa Dugger and Dr. Carlos Arteaga for providing cell lines and for their expertise in cell culture. I would like to thank Dr. Melissa Skala and all of the members of the Skala Lab for their feedback and support. Finally, I would like to thank Elvin Park for his invaluable help with cell culture and cell assays.

TABLE OF CONTENTS

Page

LIST OF TABLES

LIST OF FIGURES

CHAPTER I

INTRODUCTION

Fluorescence lifetime imaging microscopy

A fluorescence event occurs when a molecule absorbs a photon and emits a photon with less energy [1]. Photon energy is inversely related to wavelength by the equation $E = hc/\lambda$, where E represents photon energy, h refers to Planck's constant, c is the speed of light, and λ refers to wavelength. Photons emitted in a fluorescence event have a longer wavelength than the absorbed photon, and therefore emission light can be separated from excitation light using optical filters. Fluorescence microscopy takes advantage of this chemical specificity to study the properties of cells, tissues, and other samples.

Fluorescence lifetime imaging microscopy (FLIM) is a technique which probes the amount of time that a fluorophore remains in the excited state before relaxing to the ground state and emitting a photon [1, 2]. FLIM is sensitive to factors in the molecular environment of fluorophores, such as oxygen, pH, temperature, and binding to other molecules. One method of measuring the fluorescence lifetime of molecules is through time-correlated single photon counting (TCSPC), in which individual lifetime events (in the picosecond to nanosecond range) are timed, plotted as a histogram, and fit with an exponential curve (Figure 1) [3]. This exponential curve is comprised of multiple lifetime components, each of which corresponds to an individual molecular species or binding configuration of the fluorophore. TCSPC fitting determines the relative abundance of each configuration in each pixel, as well as their individual lifetimes.

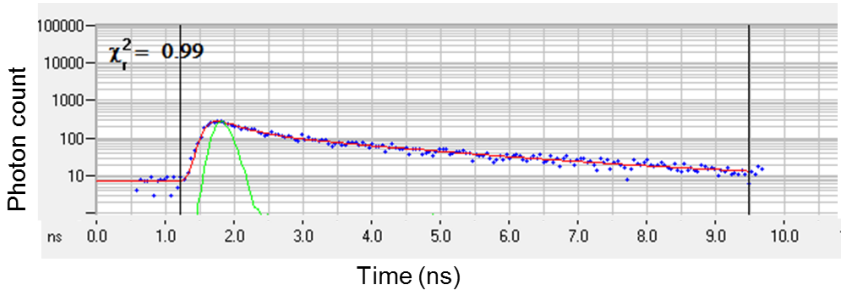

Figure 1. TCSPC fluorescence lifetime decay curve. The fluorescence lifetime in a pixel is calculated by fitting a histogram of measured lifetime events (blue) to an exponential decay function (red), after deconvolving the instrument response function (green). The chi-square value quantifies the goodness of fit.

Autofluorescence of metabolic coenzymes

Nicotinamide adenine dinucleotide (NADH) and its phosphorylated form NADPH (together referred to as NAD(P)H) are metabolic coenzymes that donate electrons to reactions. NAD(P)H, which is the reduced form of the coenzyme, is fluorescent, while the oxidized form, $NAD(P)^+$, is not. Flavin adenine dinucleotide (FAD) is another important metabolic coenzyme which is fluorescent in its oxidized form but not in its reduced form ($FADH_2$). During cellular glycolysis, NAD^+ is reduced to NADH. In oxidative phosphorylation, NADH is oxidized to NAD^+, and $FADH_2$ is oxidized to FAD. The optical redox ratio, which is defined as the ratio of the fluorescence intensity of NAD(P)H to FAD, is an established method for quantifying the metabolic state of a cell and reflects the relative amounts of glycolysis and oxidative phosphorylation being used [4-6]. Due to the Warburg effect, the preference for glycolysis exhibited by many cancer cells [7], the optical redox ratio is a particularly useful tool for exploiting intrinsic contrast to study cancer metabolism.

FLIM of NAD(P)H is a method for exploiting endogenous autofluorescence that provides complimentary information to the optical redox ratio. NAD(P)H exists in free and protein-bound states which have distinct fluorescence lifetimes [1]. Free NAD(P)H has a short lifetime due to

dynamic self-quenching by the adenine group of the molecule, while bound NAD(P)H has a long lifetime. Thus, FLIM can be used to quantify the relative abundance of each within a cell, and probe changes in cell metabolism that affect NAD(P)H binding. The lifetime of protein-bound NAD(P)H also depends on which enzyme it is bound to [8], suggesting that NAD(P)H FLIM is sensitive to changes in cell metabolism that affect the distribution of NAD(P)H binding to various enzymes.

Multiphoton microscopy

Imaging using multiphoton microscopy involves exciting a fluorophore with two or more photons simultaneously. For example, two-photon excitation involves the absorbance of two photons that each have half the energy, or twice the wavelength, of a photon required for single photon excitation [9]. Since this simultaneous absorbance of two half-energy photons is required for fluorescence excitation, the amount of photon flux needed only occurs at the focal point of the microscope objective. This eliminates excitation of fluorophores outside of the focal plane and provides very precise optical sectioning. Most endogenous fluorophores are excited by one photon of ultraviolet to visible light, or two photons of near-infrared light. Near-infrared light exhibits less scattering and absorption in tissue, and therefore two-photon excitation allow for deeper imaging penetration [10].

CHAPTER II

FLUORESCENCE LIFETIME IMAGING OF NAD(P)H DISTINGUISHES PATHWAYS OF METABOLIC INHIBITION

Introduction

Reduced nicotinamide adenine dinucleotide, or NAD(P)H, is an autofluorescent metabolic coenzyme which binds to metabolic enzymes and donates electrons to reactions in cells. The intrinsic fluorescence of NAD(P)H is useful for probing the redox state of cells due to its role in both glycolytic and oxidative phosphorylation pathways [11, 12]. In particular, optical imaging of NAD(P)H autofluorescence is ideal for monitoring cell metabolism because it is nondestructive and does not require exogenous labeling. An established method of metabolic imaging using NAD(P)H is the optical redox ratio, which is the ratio of the fluorescence intensity of NAD(P)H to that of flavin adenine dinucleotide (FAD), another autofluorescent metabolic coenzyme. NAD(P)H is produced in glycolysis and consumed in oxidative phosphorylation, while FAD is produced during oxidative phosphorylation. Thus, the ratio of their intensities provides a quantitative readout of overall cell metabolic phenotype [4]. The optical redox ratio is a proven method for probing cellular metabolism and has been harnessed for a number of applications including distinguishing cancer subtypes, monitoring cancer treatment response, and distinguishing precancerous cells from normal cells [5, 6, 13]. An increased redox ratio is often present in malignant cells because they exhibit the Warburg effect, or an excessive use of anaerobic glycolysis even in the presence of oxygen [7].

The fluorescence lifetime of NAD(P)H, or the time NAD(P)H remains excited before

relaxing back to the ground state and emitting a photon, provides additional information to the optical redox ratio regarding protein binding activity. The fluorescence lifetime of free NAD(P)H is distinctly shorter than that of protein-bound NAD(P)H due to its ability to fold on itself, causing self-quenching of the fluorescent nicotinamide ring by the adenine moiety [1]. Due to these distinct lifetimes, FLIM can quantify the amounts of free and bound NAD(P)H in the cell. Like the optical redox ratio, FLIM of endogenous fluorophores such as NAD(P)H have been used to study the role of cellular metabolism in disease pathology and progression, and as a tool for measuring cellular metabolic response to therapy [14-16]. FLIM of NAD(P)H has been applied to cell culture [5, 17-19], animal models of disease progression [13, 20, 21], and in pilot studies in human tissues both *in vivo* [22-24] and *ex vivo* [25-27]. Two-photon excitation of NAD(P)H for FLIM with near-infrared light is used in this study because it overcomes many of the difficulties caused by one-photon excitation with UV light, namely fluorophore photobleaching, photodamage to samples, and significant light scattering and absorption in tissues [28].

There is some evidence attributing NAD(P)H FLIM data to specific molecular origins. Stringari et al. found that increases in oxidative conditions such as oxidative phosphorylation shift FLIM signatures towards lower ratios of free/bound NAD(P)H in cells, while increases in reducing conditions such as glycolysis shift FLIM signatures towards higher ratios [29]. This was further supported by showing that undifferentiated stem cells, which are known to have a glycolytic phenotype, exhibit higher ratios of free/bound NAD(P)H, while differentiated stem cells exhibit a lower ratio and are known to rely primarily on oxidative phosphorylation. Maltas et al. used nanosecond-gated spectroscopy and spectral phasor analysis to identify changes in protein-bound NAD(P)H conformations associated with specific metabolic pathways [30]. They showed that their imaging system was able to distinguish between the effects of cyanide and ethanol in yeast

cells, despite the fact that they are both inhibitors of NAD(P)H oxidation. These results suggested that the redistribution of protein-bound NAD(P)H conformations caused by distinct pathways of inhibition are measurable using time-resolved optical methods. While these studies are important for interpreting NAD(P)H FLIM data, they do not look at the individual lifetime components to precisely describe changes in NAD(P)H binding activity.

While many studies have used FLIM of NAD(P)H to distinguish and quantify free and bound conformations of NAD(P)H, other studies have suggested that this may be an oversimplified interpretation, and that there may be multiple conformations of bound NAD(P)H that can be distinguished. Yaseen et al. used two-photon FLIM of NAD(P)H in exposed rat cortices to identify four distinct lifetime components, which they attribute to NAD(P)H binding to different enzymes involved in glycolysis or oxidative phosphorylation [31]. Vishwasrao et al. combined fluorescence decay and anisotropy decay information to distinguish between free NAD(P)H and three distinct species of bound NAD(P)H in rat hippocampal slices which exhibit distinct responses to anoxia [32]. Niesner et al. found that in FLIM images of human dermal fibroblasts, a wide range of bound NAD(P)H lifetimes (1-4 ns) were found across all of the pixels [33]. Protein-NAD(P)H complexes with different lifetimes within this range were not uniformly distributed across cells, but were instead found to be concentrated in certain regions, indicating that the lifetimes may be specific to different proteins. Blacker et al. studied the effects of metabolic inhibitors in cells to conclude that the bound lifetime of NAD(P)H reflects NADPH/NADH balance [34]. These studies demonstrate that a method for interpreting this complicated NAD(P)H conformational information would provide an invaluable biomarker for metabolic research.

This study tests the hypothesis that NAD(P)H FLIM is able to distinguish between different mechanisms of metabolic alteration. First, this was tested in solution. Solutions of NADH mixed

with varying ratios of malate dehydrogenase (MDH) to lactate dehydrogenase (LDH) were used to simulate cell cytoplasms in distinct metabolic states and were analyzed with FLIM. Next, the effects of two molecular inhibitors, dichloroacetate (DCA) and FX11, which are being studied as cancer therapeutics that promote oxidative phoshporylation [35-37], were measured in cells using NAD(P)H FLIM, and compared to other methods of metabolic analysis including the optical redox ratio, metabolite analysis, and cell viability analysis. The BT474 human breast cancer cell line and the MCF10A non-cancerous human breast cell line were used for this investigation in order to determine if drug effects and NAD(P)H FLIM sensitivity were cancer specific.

Materials and methods

Cell culture

BT474 cells were grown in DMEM (Invitrogen) supplemented with 10% fetal bovine serum (Invitrogen) and 1% penicillin/streptomycin (Invitrogen). MCF10A cells were grown in DMEM/F-12 (Invitrogen) supplemented with 5% horse serum (Invitrogen), 20 ng/mL EGF (Peprotech), 0.5 mg/mL hydrocortisone (Sigma), 100 ng/mL cholera toxin (Sigma), 10 μg/mL insulin (Sigma), and 1% penicillin/streptomycin (Invitrogen).

For imaging, both cell lines were seeded 24 hours prior to drug treatment in 35mm glass-bottom dishes (MatTek Corp). BT474 cells were plated at a density of $3x10^5$ cells per dish, and MCF10A cells were plated at a density of $1x10^5$ cells per dish. After 24 hours, media was replaced with either standard media, media with 1% DMSO, media with 10 μM FX11 in 1% DMSO (EMD Millipore), or media with 50 mM DCA (Sigma). 48 hours after this treatment, cells were imaged at three different locations in each plate for a total of 100-300 cells imaged per plate.

Lactate production and viability assays

BT474 cells were seeded into 96-well plates at a density of $3x10^4$ cells/well, and MCF10A cells were seeded at a density of $1x10^4$ cells/well 24 hours before drug treatment. Cells were treated with drug/vehicle for 48 hours. All media was then exchanged with serum-free media containing drug/vehicle 4 hours prior to lactate measurement. An L-Lactate Assay Kit (Eton Bioscience) was then performed on 3 wells per treatment group/cell type as well as on fresh cell media. The amount of lactate measured was averaged for each group of wells. A CellTiter-Blue Cell Viability Assay (Promega) was performed in parallel to the lactate assay to account for differences in cell number. The relative cell viability vs. control was calculated for each treatment group, and lactate production was divided by relative cell viability for each group. All assays were performed in triplicate to verify reproducibility.

Fluorescence imaging

Fluorescence intensity and lifetime images were acquired using a custom-built multiphoton fluorescence lifetime system (Bruker), with a 40x oil-immersion objective (1.3 NA and an inverted microscope (TiE, Nikon). A titanium:sapphire laser (Chameleon Ultra II, Coherent) was tuned to 750 nm for two-photon excitation of NAD(P)H and tuned to 890 nm for two-photon excitation of FAD. A 440/80nm bandpass filter was used to collect NAD(P)H fluorescence emission, and a 550/100nm was used to collect FAD emission. A pixel dwell time of 4.8 μs was used to collect images that were 256x256 pixels, with a total integration time of 60 seconds. A GaAsP PMT (H7422P-40, Hamamatsu) detected emitted photons. The field of view acquired was 270 μm x 270 μm. Time-correlated single photon counting electronics (SPC-150, Becker and Hickl) were used to acquire fluorescence decay curves. The second harmonic generated signal from urea crystals at

900 nm excitation was used to measure the instrument response function, which was found to have a full width at half maximum of 220 ps.

Cellular image analysis

A histogram of photon counts per temporal bin was constructed for each pixel in the image and then deconvolved with the instrument response function. They were then fit to a two-component exponential decay using SPCImage software (Becker & Hickl) according to equation (1), where *I(t)* represents the fluorescence intensity measured at time t after the laser pulse, α_1 and α_2 represent the fractional contributions of the short and long lifetime components to the overall intensity, respectively, τ_1 and τ_2 represent the fluorescence lifetimes of the short and long lifetime components, respectively, and *C* represents a constant level of background light.

$$I(t) = \alpha_1 exp^{-t/\tau_1} + \alpha_2 exp^{-t/\tau_2} + C \quad (1)$$

An automated cell segmentation routine was written using CellProfiler to identify individual cell cytoplasms and extract average fluorescence intensity and fluorescence lifetime values for each cell in the field of view. Optical redox ratio values were calculated for each cell by dividing the average intensity of NAD(P)H by the average intensity of FAD. For each imaging endpoint, values for all of the cells in a dish were averaged together. Dishes were generated and imaged in triplicate for each cell type and drug treatment group to generate standard error values. An unpaired t-test with Welch's correction was performed for all comparisons of imaging values.

FLIM Phasor Analysis

The sine and cosine transformations of the fluorescence decay curve were used to generate the S and G coordinates for each cytoplasm pixel within an image [38]. The mean and standard

deviation of S and G were calculated from a representative image in each treatment group.

Enzyme solutions

Tris-buffered saline at pH 7.6 was used as the solvent for all solutions. Varying concentrations of LDH from porcine heart (Sigma) or MDH from porcine heart (Sigma) were mixed with 50 μM NADH (Sigma) in order to generate solutions with distinct free-to-bound ratios of NADH. A solution of only NADH was also imaged. Four mixtures of 50 μM NADH with both LDH and MDH were generated with varying amounts of the two enzymes as described in Table 1.

Table 1. Concentrations of NADH-binding enzymes added to mixtures.

	Mixture 1	**Mixture 2**	**Mixture 3**	**Mixture 4**
[LDH] (μM)	4.9	14.2	1.4	10.0
[MDH] (μM)	13.0	2.6	13.0	8.0

Following mixing, a 100 μl droplet of each solution was placed in a separate 35 mm glass-bottom imaging dish, and a glass coverslip was placed over each droplet to reduce evaporation. Fluorescence imaging was performed as described for cells, but without FAD imaging and with an extended 120 second integration time. SPCImage was used to analyze the collected fluorescence decay curves. There is no need for high spatial resolution when imaging homogenous solutions, thus, spatial binning was used to improve fitting accuracy. For all solutions, τ_1 was fixed at 450 ps, based on the measured lifetime value of a pure NADH solution. For solutions with two enzymes, τ_1 was fixed at 450 ps, τ_2 was fixed at 1.2 ns (to represent NADH bound to MDH) and τ_3 was fixed at 1.6 ns (to represent NADH bound to LDH). A regression line with y-intercept fixed

at 0 was calculated for the relationship between the relative amount of LDH in a solution of NADH, LDH, and MDH, and its relative measured α value. A 95% confidence interval for this line was calculated, along with its coefficient of determination and p-value.

Results

FLIM of NADH-enzyme binding

The lifetimes of NADH bound to metabolic enzymes in solution were measured. Solutions of 50 μM NADH were mixed with varying amounts of either LDH (Figure 1A,C) or MDH (Figure 1B,D) and imaged using FLIM. This resulted in mixtures with a range of values for the fraction of free NADH, or α_1 as measured with FLIM. The measured value for the bound lifetime of NADH, or τ_2, did not change with enzyme concentration, and was found to be about 1.2 ns for NADH bound to MDH and 1.6 ns for NADH bound to LDH. Next, four solutions of 50 μM NADH were mixed with varying amounts of both MDH and LDH and imaged. The relative amount of LDH added to a mixture of NADH, LDH, and MDH, and its relative measured α value correlated strongly ($R^2 = 0.9842$, $p<0.01$, Figure 1E).

Drug effects on cancer cells

The effects of 48 hours of treatment with either DCA or FX11 on the optical redox ratio were evaluated in BT474 and MCF10A cells (Figure 2A-H). Both drugs were found to cause a significant decrease in the redox ratio both visually and statistically in both cell types versus controls ($p<0.05$), which suggests a shift from glycolysis to oxidative phosphorylation as the preferred metabolic pathway as a result of treatment [4, 13]. To further understand the metabolic

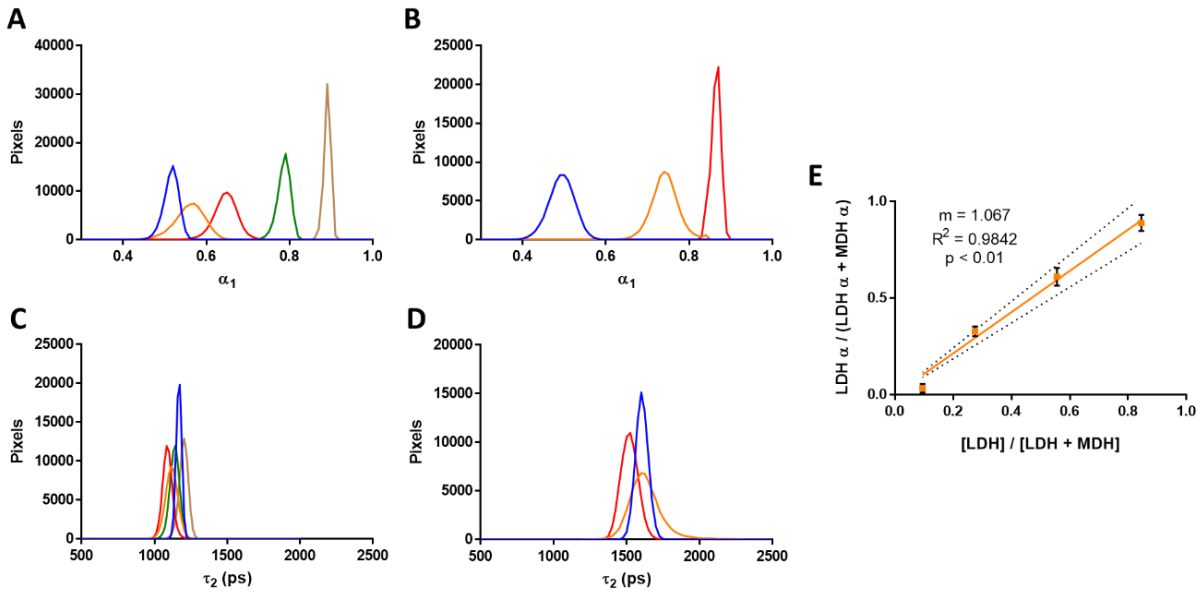

Figure 2. Metabolic enzyme solutions. The fraction of free NADH, or α_1, was measured in mixtures of 50 μM NADH with varied concentrations of (A) MDH or (B) LDH. Histograms were generated of all the pixels in a single image to show the distribution of values. The bound lifetime of NADH, or τ_2, was measured in the same solutions (C,D) and shown with histograms of corresponding colors. The relationship between the relative amount of LDH in a solution of NADH, LDH, and MDH, and its relative measured α value are depicted in (E). Error bars represent the standard deviation across all the pixels in an image, and the dotted line represents the 95% confidence interval for the regression line.

pathways affected by these drugs, lactate production was measured after 48 hours of drug or vehicle treatment (Figure 2I-L). FX11 was found to cause a significant increase in lactate production when adjusted for relative cell viability ($p<0.05$) versus vehicle, while DCA caused a significant decrease versus vehicle ($p<0.05$).

Drug effects on FLIM of NAD(P)H

The effects of 48 hours of treatment with either DCA or FX11 on the fluorescence lifetime of NAD(P)H, specifically the bound lifetime τ_2, were evaluated in BT474 and MCF10A cells (Figure 3A-H). FX11 caused a significant decrease in NAD(P)H τ_2 in both BT474 and MCF10A

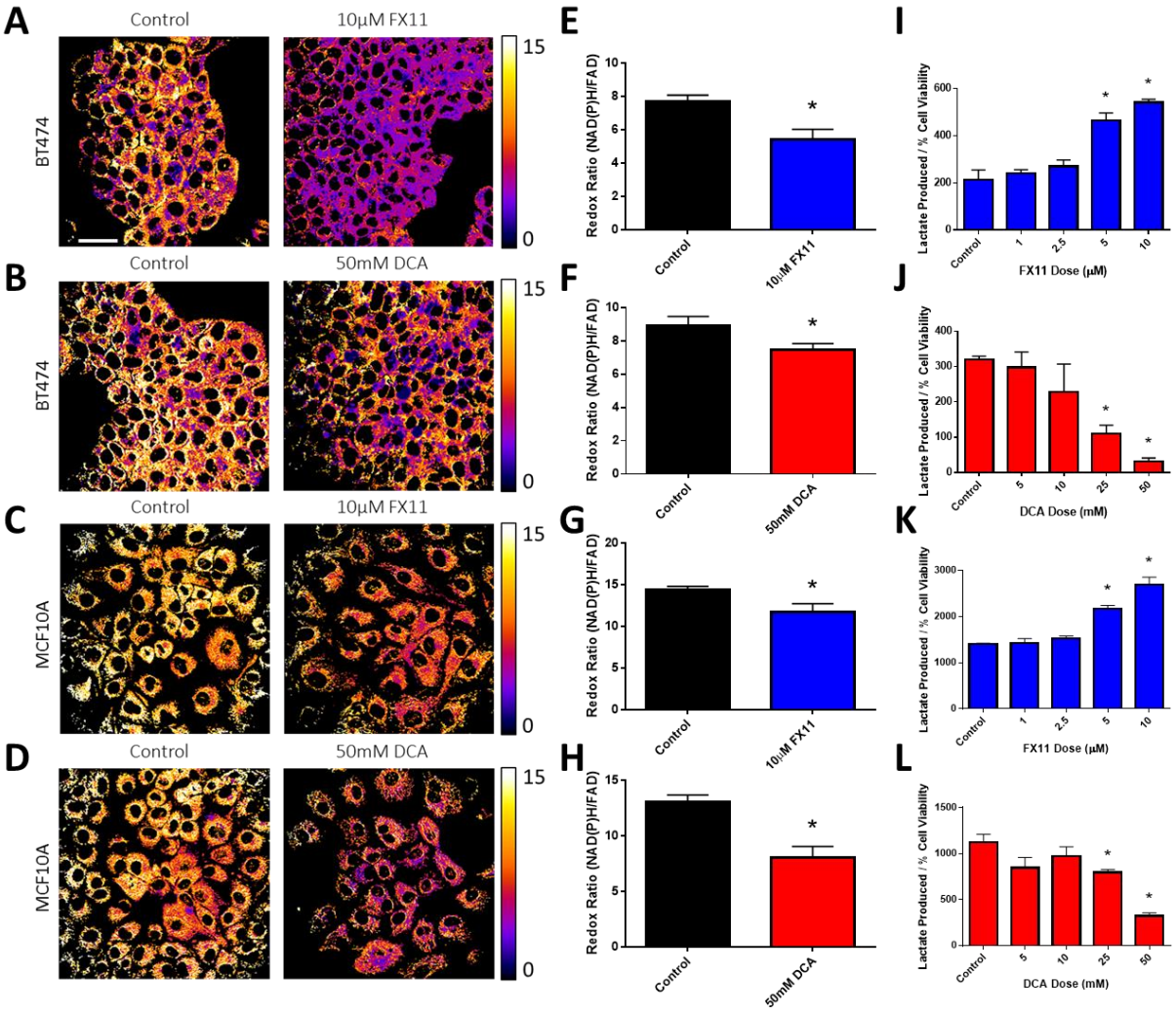

Figure 3. Drug effects on redox ratio and lactate production. (A-D) Representative images of both cell types after 48 hours of drug or vehicle treatment, color-coded for the redox ratio. Scale bar is 50 μm. (E-H) Mean and standard deviations of the redox ratios before and after 48 hours of drug or vehicle treatment. * $p<0.05$ vs. control. n = 3 experiments. (I-L) Dose-response of lactate production controlled for relative cell viability after 48 hours of drug or vehicle treatment. * $p<0.05$ vs. control. n = 3 wells.

cells versus vehicle ($p<0.05$) while DCA did not cause a significant change in NAD(P)H τ_2 versus vehicle. Phasor analysis of the cytoplasm pixels in the representative images (Figure 3I-L) further demonstrate that a shift is occurring in the fluorescence lifetime of NAD(P)H as a result of FX11 treatment, but not DCA treatment.

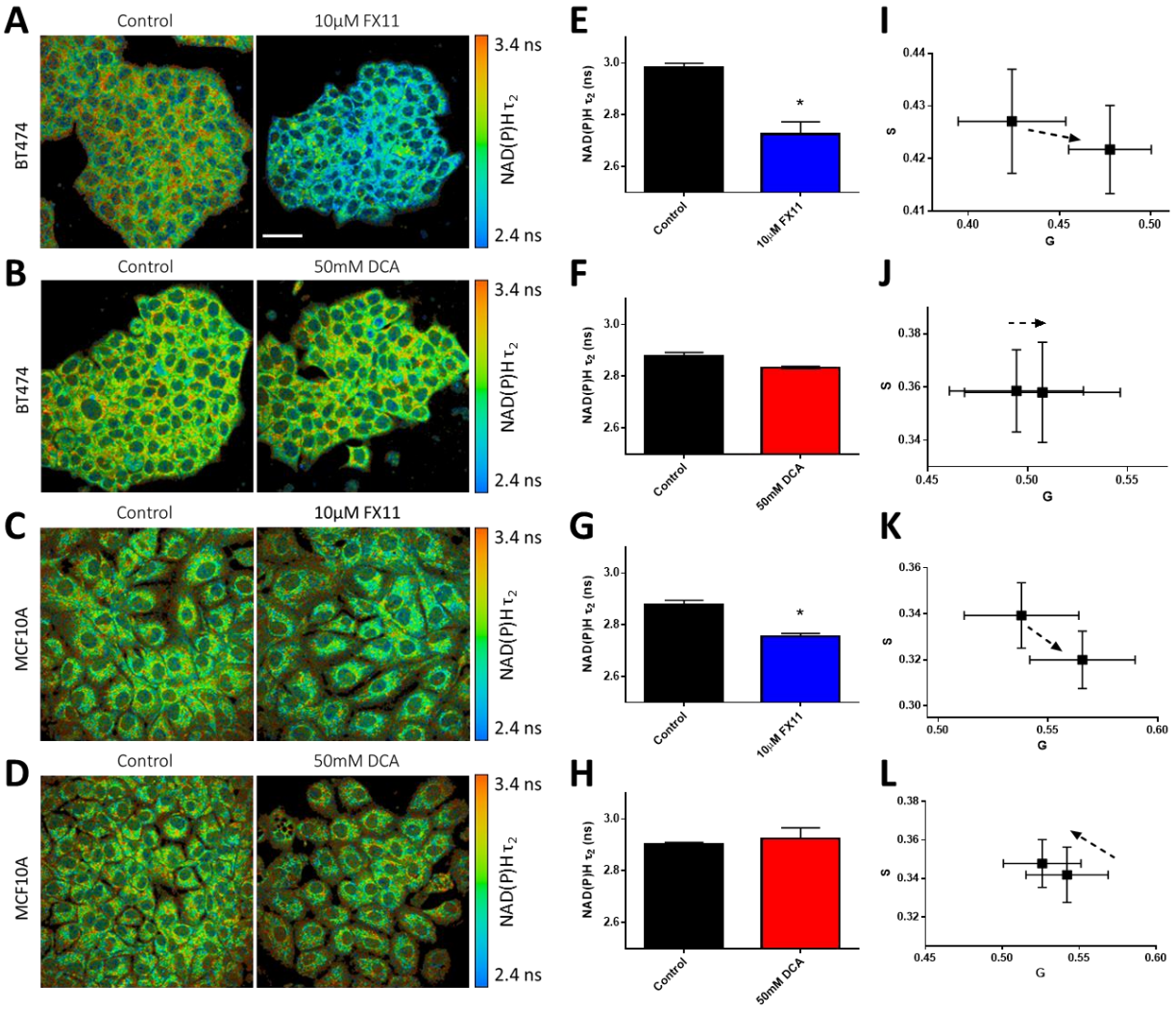

Figure 4. Drug effects on FLIM of NAD(P)H. (A-D) Representative images of both cell types after 48 hours of drug or vehicle treatment, color-coded for NAD(P)H τ_2. Scale bar is 50 μm. (E-H) Mean and standard deviations of the NAD(P)H τ_2 before and after 48 hours of drug or vehicle treatment. * $p<0.05$ vs. control. n = 3 dishes. (I-L) Mean and standard deviation of the phasor coordinates of the cytoplasm pixels from the representative images. Dotted arrows represent shift from vehicle-treated cells to drug-treated cells.

Table 2 summarizes how these two drugs affect both imaging and non-imaging parameters in both of the cell lines investigated. Effects on lactate production, redox ratio, and NAD(P)H τ_2 represent statistically significant shifts based on results shown here, while effects on oxygen consumption represent previously published results in other cancer cell types.

Table 2. Summary of drug effects in MCF10A and BT474 cells

	Dichloroacetate	**FX11**
O_2 consumption [35-37]	↑	↑
Lactate production	↓	↑
Redox ratio	↓	↓
NAD(P)H τ_2	No effect	↓

Discussion

Fluorescence lifetime imaging of autofluorescent NAD(P)H is a useful technique for non-invasively monitoring changes in cellular metabolic activity due to its sensitivity to shifts in the molecular conformation of NAD(P)H. There has been a significant desire in the field to robustly describe the relationship between NAD(P)H lifetime parameters and specific metabolic events within cells. In order to leverage NAD(P)H FLIM as an optical biomarker for drug screening technology and metabolic research, a strong understanding of this relationship is required. To date, NAD(P)H fluorescence lifetime data has often been analyzed with a binary system of interpretation, where NAD(P)H has either a short or long fluorescence lifetime depending on whether it is in a free or protein-bound state [4]. Some evidence has been found that may suggest biochemical interpretations of NAD(P)H lifetime data, such as an increase in the ratio of free to bound NAD(P)H being attributed to an increase in glycolysis vs. oxidative phosphorylation, and vice versa [29].

We hypothesized that NAD(P)H lifetime data could be even more precisely attributed to specific cellular metabolic events. There are a number of metabolic events that could lead a cell to shift its preference for glycolysis or oxidative phosphorylation, and we believed that these factors could be distinguished if they had unique and measurable effects on the activities of enzymes

which bind NAD(P)H in the cell. First, we wanted to determine whether FLIM of NAD(P)H could accurately quantify the degree to which NAD(P)H is binding to individual metabolic enzymes within a mixture. We chose to measure this in solutions with a variety of LDH and MDH concentrations in order to model what takes place in a cell when flux through individual metabolic pathways are activated or inhibited in response to external stimuli. We show that indeed, FLIM of NAD(P)H using two-photon excitation can accurately quantify the relative amounts of NAD(P)H bound to each individual metabolic enzyme in a mixture (Figure 1E). This *in vitro* model of metabolic activity in the cell cytoplasm is very simplified, but it demonstrates the ability of this imaging technique to measure the relative NAD(P)H binding to multiple enzymes if the individual lifetimes are known and are sufficiently distinct. These results suggest that in cells, this technology could be used to track the activation and inhibition of individual metabolic pathways that bind NAD(P)H.

In order to determine whether fluorescence lifetime imaging of NAD(P)H could distinguish between unique shifts in flux through metabolic pathways in cells, the effects of two metabolic inhibitors were investigated. DCA and FX11 were chosen because they were both expected to drive cells towards using more oxidative phosphorylation and less glycolysis [35-37], and to do so by different mechanisms and thus have unique effects on metabolic pathways. Our optical redox ratio results suggest that indeed, these drugs promote oxidative phosphorylation in both malignant (BT474) and non-malignant (MCF10A) human breast cell lines (Figure 2E-H). Our lactate production results also support the notion that these two drugs exert their effects on metabolism through different metabolic pathways and enzymes. While FX11 causes a significant increase in lactate production per cell ($p<0.05$, Figure 2I,K), DCA was found to cause a significant decrease ($p<0.05$, Figure 2J,L), despite the fact that both resulted in the same overall shift in metabolic

phenotype towards oxidative phosphorylation. These results also determined the doses of these drugs to use in our imaging studies in order to cause significant metabolic change in these cell lines (50 mM DCA and 10 μM FX11).

Once we verified that these drugs had unique effects on cellular metabolic enzyme activity, we determined whether fluorescence lifetime imaging of NAD(P)H was able to distinguish between the two. Indeed, we found that the bound lifetime of NAD(P)H, τ_2, was sensitive to the significant shifts in metabolic enzyme activity caused by FX11 ($p<0.05$, Figure 3E,G), but not DCA (Figure 3F,H). SPCImage software uses a least squares method with iterative re-convolution to determine these fluorescence decay parameters, which requires a priori estimation of the number of fluorescent species in a sample [3]. In order to confirm these results by a secondary method that does not use multiexponential fitting, phasor analysis of our NAD(P)H FLIM data was performed (Figure 3I-L). This analysis confirmed that 48 hours of FX11 treatment in both cell types causes a significant shift in the distribution of phasors within acquired images, while DCA treatment does not. In total, these results suggest that FLIM of NAD(P)H has variable sensitivity to different shifts in enzyme binding activity that cause the same shift in overall cell metabolism. The reason for this differential sensitivity could be that in these cells, DCA shifts metabolic enzymes in a manner which does not have a detectable effect on NAD(P)H binding, either because affected enzymes do not bind large amounts of NAD(P)H, or because NAD(P)H preferred protein binding shifts between two or more metabolic enzymes that give similar NAD(P)H bound lifetimes.

In order to relate NAD(P)H lifetime data to more specific metabolic events, future work will involve directly measuring enzyme-NAD(P)H binding activities and correlating them to FLIM measurements. For example, ^{13}C-labeling of metabolic substrates and mass spectrometry could be used to measure the flux through individual metabolic pathways and quantify the relative activities

of various enzymes which bind NAD(P)H [39]. A model which was able to relate NAD(P)H FLIM data to shifts in the activity of specific NAD(P)H-binding enzymes would prove invaluable for the development of NAD(P)H FLIM as a tool for metabolic research and as a biomarker for therapeutic response in cancer. Instead of analyzing NAD(P)H FLIM data as a simple free vs. bound system with two exponential decays, future analysis could include contributions from free NAD(P)H as well as NAD(P)H bound to each individual metabolic enzyme of interest. By looking at these individual bound lifetimes instead of a mean bound lifetime value, metabolic flux data could be extracted. Such a model could allow physicians to quickly and non-invasively elucidate the pathways of resistance that are responsible for failing drug treatments in individual cancer patients, and predict response to alternative treatment options.

Chapter III

CONCLUSION AND FUTURE DIRECTIONS

This study demonstrates that FLIM of NAD(P)H is able to accurately quantify the relative amounts of LDH-NADH and MDH-NADH binding in a single solution *in vitro*, suggesting that this technology could be extended to cells to measure preferred protein binding by NAD(P)H. BT474 cells and MCF10A cells both exhibited a decrease in optical redox ratio pointing towards an increase in oxidative phosphorylation when treated with metabolic inhibitors DCA and FX11. In both cell types, DCA causes a decrease in lactate production per cell, while FX11 causes an increase, suggesting that these two drugs affect different metabolic pathways. FLIM of NAD(P)H shows sensitivity to the shifts in NAD(P)H-enzyme binding caused by FX11, but not DCA. These results suggest that FLIM of NAD(P)H could be developed as a tool for differentiating between specific shifts in metabolic enzyme activities and quantifying flux through metabolic pathways.

Future work is necessary to more specifically attribute changes in NAD(P)H bound lifetime to changes in the activity of metabolic enzymes that bind NAD(P)H. This could be achieved by systematically activating and inhibiting key metabolic enzymes in cells using targeted drugs or siRNAs, and measuring the effects they have on NAD(P)H bound lifetimes. Metabolic flux analysis could be used as a gold standard to quantify inhibition and activation of metabolic pathways. This technology would have a number of applications in metabolic research, cancer biology, and drug development.

REFERENCES

1. Lakowicz, J.R., *Principles of fluorescence spectroscopy*. 2nd ed. 1999, New York: Kluwer Academic/Plenum. xxiii, 698 p.
2. Lakowicz, J.R., et al., *Fluorescence lifetime imaging of free and protein-bound NADH.* Proc Natl Acad Sci U S A, 1992. **89**(4): p. 1271-5.
3. Becker, W., *Advanced time-correlated single photon counting techniques*. Springer series in chemical physics,. 2005, Berlin ; New York: Springer. xix, 401 p.
4. Chance, B., et al., *Oxidation-reduction ratio studies of mitochondria in freeze-trapped samples. NADH and flavoprotein fluorescence signals.* J Biol Chem, 1979. **254**(11): p. 4764-71.
5. Walsh, A.J., et al., *Optical metabolic imaging identifies glycolytic levels, subtypes, and early-treatment response in breast cancer.* Cancer Res, 2013. **73**(20): p. 6164-74.
6. Ostrander, J.H., et al., *Optical redox ratio differentiates breast cancer cell lines based on estrogen receptor status.* Cancer Res, 2010. **70**(11): p. 4759-66.
7. Warburg, O., *On the origin of cancer cells.* Science, 1956. **123**(3191): p. 309-14.
8. Iweibo, I., *Protein fluorescence and electronic energy transfer in the determination of molecular dimensions and rotational relaxation times of native and coenzyme-bound horse liver alcohol dehydrogenase.* Biochim Biophys Acta, 1976. **446**(1): p. 192-205.
9. Denk, W., J.H. Strickler, and W.W. Webb, *Two-photon laser scanning fluorescence microscopy.* Science, 1990. **248**(4951): p. 73-6.
10. Helmchen, F. and W. Denk, *Deep tissue two-photon microscopy.* Nat Methods, 2005. **2**(12): p. 932-40.
11. Heikal, A.A., *Intracellular coenzymes as natural biomarkers for metabolic activities and mitochondrial anomalies.* Biomark Med, 2010. **4**(2): p. 241-63.
12. Uppal, A. and P.K. Gupta, *Measurement of NADH concentration in normal and malignant human tissues from breast and oral cavity.* Biotechnol Appl Biochem, 2003. **37**(Pt 1): p. 45-50.
13. Skala, M.C., et al., *In vivo multiphoton microscopy of NADH and FAD redox states, fluorescence lifetimes, and cellular morphology in precancerous epithelia.* Proc Natl Acad Sci U S A, 2007. **104**(49): p. 19494-9.
14. Conklin, M.W., et al., *Fluorescence lifetime imaging of endogenous fluorophores in histopathology sections reveals differences between normal and tumor epithelium in carcinoma in situ of the breast.* Cell Biochem Biophys, 2009. **53**(3): p. 145-57.
15. Walsh, A.J., et al., *Quantitative optical imaging of primary tumor organoid metabolism predicts drug response in breast cancer.* Cancer Res, 2014. **74**(18): p. 5184-94.
16. Ghukasyan, V.V. and F.J. Kao, *Monitoring Cellular Metabolism with Fluorescence Lifetime of Reduced Nicotinamide Adenine Dinucleotide.* Journal of Physical Chemistry C, 2009. **113**(27): p. 11532-11540.
17. Bird, D.K., et al., *Metabolic mapping of MCF10A human breast cells via multiphoton fluorescence lifetime imaging of the coenzyme NADH.* Cancer Res, 2005. **65**(19): p. 8766-73.
18. Walsh, A., et al., *Optical imaging of metabolism in HER2 overexpressing breast cancer cells.* Biomed Opt Express, 2012. **3**(1): p. 75-85.

19. Guo, H.W., et al., *Reduced nicotinamide adenine dinucleotide fluorescence lifetime separates human mesenchymal stem cells from differentiated progenies.* J Biomed Opt, 2008. **13**(5): p. 050505.
20. Walsh, A.J., et al., *Ex vivo optical metabolic measurements from cultured tissue reflect in vivo tissue status.* J Biomed Opt, 2012. **17**(11): p. 116015.
21. Cheng, S., et al., *Handheld multispectral fluorescence lifetime imaging system for in vivo applications.* Biomed Opt Express, 2014. **5**(3): p. 921-31.
22. Sun, Y., et al., *Simultaneous time- and wavelength-resolved fluorescence spectroscopy for near real-time tissue diagnosis.* Opt Lett, 2008. **33**(6): p. 630-2.
23. Meier, J.D., et al., *Time-resolved laser-induced fluorescence spectroscopy as a diagnostic instrument in head and neck carcinoma.* Otolaryngol Head Neck Surg, 2010. **142**(6): p. 838-44.
24. Butte, P.V., et al., *Intraoperative delineation of primary brain tumors using time-resolved fluorescence spectroscopy.* J Biomed Opt, 2010. **15**(2): p. 027008.
25. Dimitrow, E., et al., *Spectral fluorescence lifetime detection and selective melanin imaging by multiphoton laser tomography for melanoma diagnosis.* Exp Dermatol, 2009. **18**(6): p. 509-15.
26. Galletly, N.P., et al., *Fluorescence lifetime imaging distinguishes basal cell carcinoma from surrounding uninvolved skin.* Br J Dermatol, 2008. **159**(1): p. 152-61.
27. Kennedy, G.T., et al., *A fluorescence lifetime imaging scanning confocal endomicroscope.* J Biophotonics, 2010. **3**(1-2): p. 103-7.
28. Huang, S., A.A. Heikal, and W.W. Webb, *Two-photon fluorescence spectroscopy and microscopy of NAD(P)H and flavoprotein.* Biophys J, 2002. **82**(5): p. 2811-25.
29. Stringari, C., et al., *Phasor fluorescence lifetime microscopy of free and protein-bound NADH reveals neural stem cell differentiation potential.* PLoS One, 2012. **7**(11): p. e48014.
30. Maltas, J., et al., *Autofluorescence from NADH Conformations Associated with Different Metabolic Pathways Monitored Using Nanosecond-Gated Spectroscopy and Spectral Phasor Analysis.* Anal Chem, 2015. **87**(10): p. 5117-24.
31. Yaseen, M.A., et al., *In vivo imaging of cerebral energy metabolism with two-photon fluorescence lifetime microscopy of NADH.* Biomed Opt Express, 2013. **4**(2): p. 307-21.
32. Vishwasrao, H.D., et al., *Conformational dependence of intracellular NADH on metabolic state revealed by associated fluorescence anisotropy.* J Biol Chem, 2005. **280**(26): p. 25119-26.
33. Niesner, R., et al., *Noniterative biexponential fluorescence lifetime imaging in the investigation of cellular metabolism by means of NAD(P)H autofluorescence.* Chemphyschem, 2004. **5**(8): p. 1141-9.
34. Blacker, T.S., et al., *Separating NADH and NADPH fluorescence in live cells and tissues using FLIM.* Nat Commun, 2014. **5**: p. 3936.
35. Michelakis, E.D., L. Webster, and J.R. Mackey, *Dichloroacetate (DCA) as a potential metabolic-targeting therapy for cancer.* Br J Cancer, 2008. **99**(7): p. 989-94.
36. Le, A., et al., *Inhibition of lactate dehydrogenase A induces oxidative stress and inhibits tumor progression.* Proc Natl Acad Sci U S A, 2010. **107**(5): p. 2037-42.
37. Cairns, R.A., et al., *Metabolic targeting of hypoxia and HIF1 in solid tumors can enhance cytotoxic chemotherapy.* Proc Natl Acad Sci U S A, 2007. **104**(22): p. 9445-50.

38. Digman, M.A., et al., *The phasor approach to fluorescence lifetime imaging analysis.* Biophys J, 2008. **94**(2): p. L14-6.
39. Zamboni, N., et al., *(13)C-based metabolic flux analysis.* Nat Protoc, 2009. **4**(6): p. 878-92.